Original Article

Statistical changes of lung morphology in patients with adolescent idiopathic scoliosis after spinal fusion surgery—a prospective nonrandomized study based on low-dose biplanar X-ray imaging

Min Deng[1], Qianyun Chen[1], Qiao Deng[1], Lin Shi[1], Cherry Cheuk Nam Cheng[1], Kwong Hang Yeung[1], Rongli Zhang[1], Wai Ping Fiona Yu[2], Tsz Ping Lam[2], Jack Chun Yiu Cheng[2], Winnie Chiu Wing Chu[1]

[1]Department of Imaging and Interventional Radiology, Faculty of Medicine, The Prince of Wales Hospital, The Chinese University of Hong Kong, Hong Kong, China; [2]SH Ho Scoliosis Research Laboratory, Department of Orthopaedics and Traumatology, Faculty of Medicine, The Prince of Wales Hospital, The Chinese University of Hong Kong, Hong Kong, China

Contributions: (I) Conception and design: WCW Chu, L Shi, JCY Cheng; (II) Administrative support: WCW Chu, L Shi, JCY Cheng, TP Lam; (III) Provision of study materials or patients: JCY Cheng, TP Lam, WCW Chu; (IV) Collection and assembly of data: M Deng, KH Yeung, WPF Yu, CCN Cheng; (V) Data analysis and interpretation: M Deng, Q Deng, Q Chen, R Zhang; (VI) Manuscript writing: All authors; (VII) Final approval of manuscript: All authors.

Correspondence to: Prof. Winnie Chiu Wing Chu, MD; Prof. Lin Shi, PhD. Department of Imaging and Interventional Radiology, Faculty of Medicine, The Prince of Wales Hospital, The Chinese University of Hong Kong, Shatin, Hong Kong, China.
Email: winniechu@cuhk.edu.hk; shilin@cuhk.edu.hk.

Background: Adolescent idiopathic scoliosis (AIS) patients suffer from restrictive impairment of pulmonary function (PF) as a consequence of spinal and ribcage deformity. Statistic modelling of scoliotic geometry has been well-established based on low-dose biplanar X-ray device (EOS) imaging. However, the postoperative lung morphology change derived from EOS has not yet been studied adequately till now.

Methods: Twenty-five female AIS patients with severe right-sided major thoracic curve (aged 13–31 years; Cobb angle 45°–92°) underwent posterior spinal fusion (PSF) were prospectively recruited for standing EOS imaging at preoperative, postoperative, and 1-year follow-up (1Y-FU) stages. EOS-based lung morphology at frontal and lateral view was measured respectively to assess serial statistical changes in area and height.

Results: At frontal view, left lung area significantly increased postoperatively (104.7 *vs.* 125.1 cm^2; P<0.001) but without continuous increase at 1Y-FU (125.1 *vs.* 124.5 cm^2; P=0.084), whereas right lung area showed a slight but insignificant interval increase (median: 143.8, 146.5, 148.4 cm^2 at preoperative, postoperative, 1Y-FU stage, respectively; all P>0.05). At lateral view, the increase in left lung area was slight without statistically difference (median: 175.8, 178.4, 182.5 cm^2 at preoperative, postoperative, 1Y-FU stage, respectively; all P>0.05), while right lung area did not significantly change postoperatively (median: 209.9, 206.7, 212.4 cm^2 at preoperative, postoperative, 1Y-FU stage, respectively; all P>0.05). At both frontal and lateral view, left lung height significantly improved at both postoperative and 1Y-FU stage (all P<0.05), while preoperative right lung height was not significantly different from postoperative and 1Y-FU value (all P>0.05).

Conclusions: EOS imaging demonstrates that left lung area in severe AIS may improve after PSF surgery. EOS may provide useful information about lung morphology change after PSF in severe AIS.

Keywords: Biplanar radiography; lung; idiopathic scoliosis; radiation

Submitted Nov 27, 2021. Accepted for publication Dec 27, 2021; Published online: 31 Mar 2022.
doi: 10.21037/qims-21-1147
View this article at: https://dx.doi.org/10.21037/qims-21-1147

Introduction

Adolescent idiopathic scoliosis (AIS), defined as a radiological lateral spinal curvature with Cobb angle of at least 10°, is a complex three-dimensional (3D) structural spinal deformity without definitive aetiology, occurring in 1–4% of the adolescents aged 10–16 years (1,2). Untreated AIS may lead to restrictive form of pulmonary dysfunction (3), while severe AIS is prone to pulmonary hypertension, respiratory failure and premature mortality (3,4). The reported incidence of pulmonary function (PF) impairment varies considerably in surgically treated AIS patients, which ranges from approximately 20% to 61%, according to American Thoracic Society threshold for normal PF (5-7). Diminished PF in AIS correlates with curve magnitude, number of vertebrae involved in major curve, sagittal hypokyphosis, apex displacement, rib-vertebral angle, coronal imbalance (7,8). Lung morphology assessment using non-invasive imaging provides an objective tool to monitor pulmonary impairment and rate surgical outcome.

Conventionally the 3D assessment of distorted lung heavily relies on computed tomography (CT) or magnetic resonance imaging (MRI) (3,9). Nevertheless, high radiation exposure ineluctably precludes utilization of CT as routine workup in adolescents entering the starting period of the reproductive age, especially for those requiring serial follow-up examinations. The widespread use of MRI for depicting lung anatomy, albeit radiation-free, is hindered by high cost and inherent long scanning time. Apart from that, the metallic implants in post-operative patients may induce distortion artefacts on the immediate adjacent structures like vertebral column and central canal, affecting the visualization of the lung contour. Other disadvantages shared by CT and MRI are intrinsic as results of supine position of subjects during scanning, which mainly include the underestimated scoliotic magnitude, discrepancy in vertebral rotation, incapability to fully evaluate the upright biomechanics (10-12).

The low-dose biplanar X-ray device (EOS) is a breakthrough in acquiring frontal and lateral radiographs of full body simultaneously in a standing position, with markedly lower exposure to ionizing radiation. For scoliotic curvature, EOS-based 3D modelling of spine allows the accurate 3D representations of vertebral position, orientation/rotation, and body shape (13-16). Hence, EOS tends to be a surrogate imaging tool to regularly monitor scoliotic curve progression in a physiological weight-bearing upright position. The geometric features of scoliotic vertebrae extracted from EOS have been well documented, owing to plenty of statistic or knowledge-based EOS-3D modelling, particularly those built on the large-scale cohort comprising of a thousand of non-scoliosis and scoliosis individuals (16-18). Though EOS imaging shows a potential in evaluation of serial changes of lung morphology, especially in severe AIS patients with surgical correction, EOS-derived assessment of lung morphology is not yet studied adequately thus far.

In present study, using AIS patients treated with spinal fusion surgery as a clinical sample, we sought to demonstrate the clinical applicability of EOS in lung morphology assessment, by comparing lung geometric features between pre-operative and post-operative AIS. We present the following article in accordance with the TREND reporting checklist (available at https://qims.amegroups.com/article/view/10.21037/qims-21-1147/rc).

Methods

Subjects

During the period from June 2015 to July 2017, patients diagnosed with AIS were prospectively recruited. All patients were referral in scoliosis clinic at the Prince of Wales Hospital (PWH), one of the only two tertiary referral centers specialized in scoliosis in Hong Kong. The inclusion criteria were: (I) with severe right-thoracic curves (major Cobb angle of no less than 45°); (II) scheduled to undergo spinal fusion surgery; (III) written consent provided. Exclusion criteria were: (I) neuromuscular or congenital scoliosis or any other type of spinal deformity; (II) known history of pulmonary diseases, back injury, weakness, or numbness in one or more limbs, urinary inconsistence or nocturnal enuresis; (III) conditions and medications that would affect bone remodeling and calcium metabolism, neuromuscular abnormalities, genetic diseases, chromosomal defects, autoimmune disorders, endocrine disturbances. The study was conducted in accordance with the Declaration of Helsinki (as revised in 2013). Ethical approval was obtained from The Joint Chinese University of Hong Kong-New Territories East Cluster Clinical Research Ethics Committee (CREC Ref. No. 2013.386 and No. 2016.058). Written informed consent was obtained from study patients or their parent/guardian.

The posterior spinal fusion (PSF) surgical procedure was performed on 25 subjects. All of them were free from any respiratory symptoms or acute respiratory infections

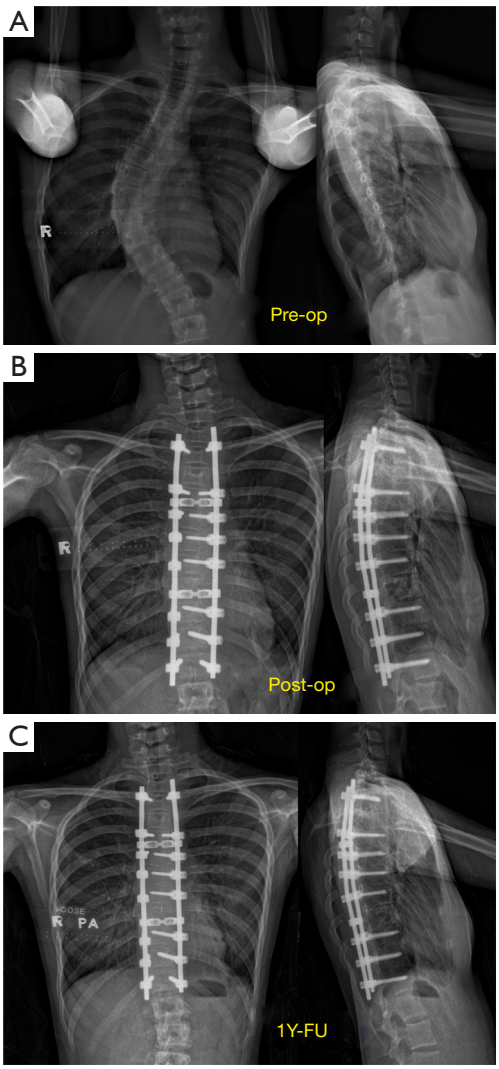

Figure 1 EOS of a 14-year-old severe AIS girl. The right-sided thoracic scoliosis (Cobb angle =61°) on preoperative images (A) is significantly reduced on postoperative (Cobb angle =18°) images (B), and 1Y-FU (Cobb angle =22°) images (C). Left column: EOS at frontal view; right column: EOS at lateral view. EOS, low-dose biplanar X-ray device; AIS, adolescent idiopathic scoliosis; 1Y-FU, 1-year follow up.

at the time of EOS studies before and after operation. Demographic and clinical data were recorded, including age at menarche, body weight, standing height, body mass index, arm span and so forth. The information of participants was available to the staff member performing the assessments.

Image acquisition

The whole body stereoradiography was performed using biplanar X-ray unit (EOS® Imaging, Paris, France) by a team of highly experienced radiographer. Each AIS patient underwent consecutive EOS at three time points: pre-operative, post-operative, and 1-year follow-up (1Y-FU) stage (*Figure 1*). The standard low-dose protocol was applied to preoperative and postoperative EOS imaging, while the micro-dose protocol was chosen for 1Y-FU EOS imaging (June 2016 to July 2018) to follow the As Low As Reasonably Practicable (ALARP) principle. The estimated effective dose of a single biplanar X-ray ranged from 220 to 290 μSv in standard low-dose protocol and from 22 to 37 μSv in micro-dose protocol (19-21). Subjects were instructed to keep a free upright position with hips and knees extended, along with both arms raised and hands holding the handling bar (22). Subjects were also required to hold breath and remain motionless during scan. The standing stereo-radiographs at frontal and lateral views were captured simultaneously without introducing digital stitching bias, by the synchronized vertical movement of two pairs of co-linked X-ray tube and slot-scanning detector, which are positioned perpendicular to each other. The average time for a full-body scan was approximately 19 s. During a regular tidal breathing cycle, respiratory amplitude remains relatively constant in each subject, indicating a similar inspiration depth of breath-holding among three EOS examinations. The highest point and the vertical excursion of diaphragm on EOS were estimated, in case of any significant difference in inspiration depth of breath-holding episodes. Cobb angle on coronal plane (frontal image) was measured to assess the change in curve magnitude at each time point.

EOS-derived lung morphology assessment

Lung contour segmentation based on EOS images

The contour of bilateral lungs was manually labelled by an experienced radiologist from frontal and lateral EOS image respectively using Insight Segmentation and Registration Toolkit (ITK) software (*Figure 2*). To test the intra-observer reliability of EOS geometric measurements, labelling for preoperative and postoperative EOS images in 10 patients were repeated by same radiologist at an interval of 4 weeks. In term of intraclass correlation coefficient (ICC) value, reliability was graded as excellent (ICC >0.9), good (0.9≥

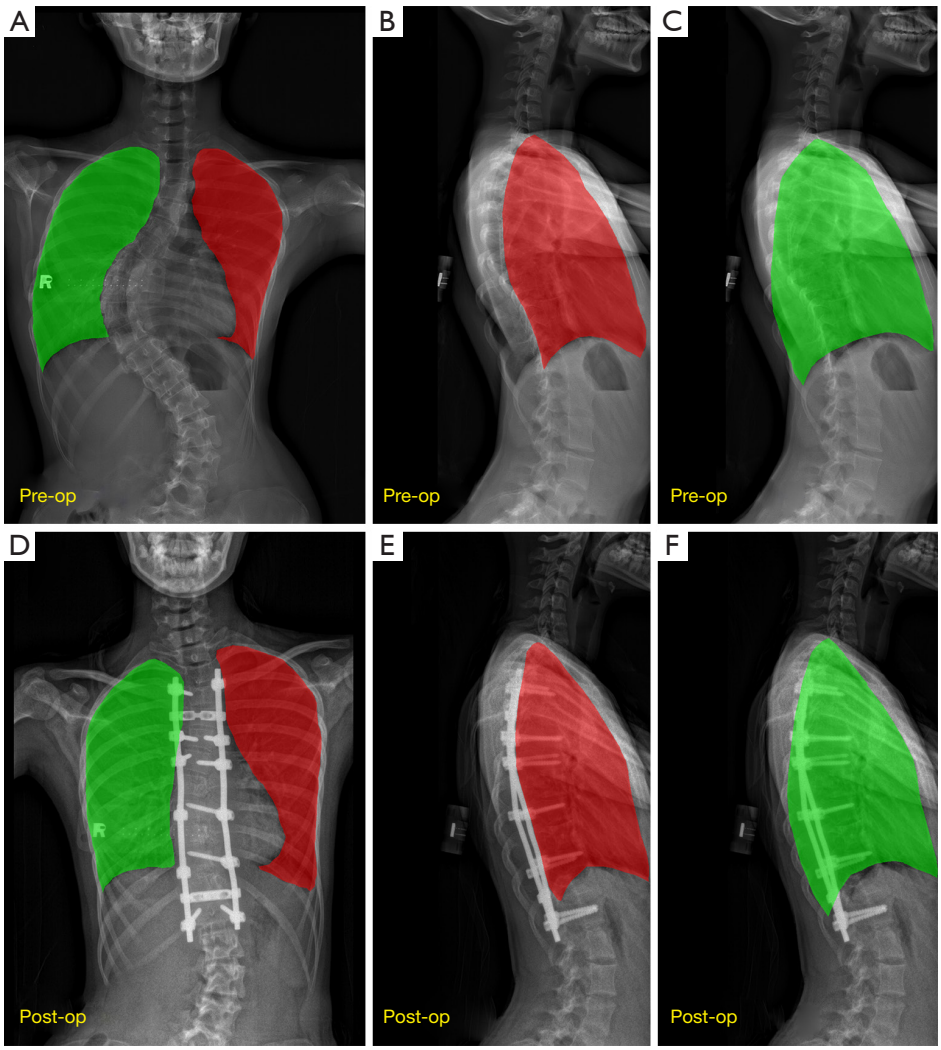

Figure 2 Lung label on EOS images. The masks of bilateral lungs at both frontal and lateral view segmented for geometric feature extraction at preoperative (A-C) and postoperative (D-F) stages. Red mask: left lung; green mask: right lung. EOS, low-dose biplanar X-ray device.

ICC ≥0.75), moderate (0.75≥ ICC ≥0.5), poor (ICC <0.5), respectively (23).

EOS-derived lung geometric measures

This step was implemented by in-house developed Python program (Python version 3.8.5 available at https://www.python.org/downloads/release/python-385/). A prior bounding box of lung contour was automatically draw over EOS image for measuring geometric features (24). Bounding box is defined by the smallest rectangle with vertical and horizontal sides that completely surrounds an object of interest (i.e., labelled lung). All portions of the labelled lung lie within the generated bounding rectangle.

At both frontal and lateral view, the geometric properties of lung were measured, consisting of: (I) lung area and perimeter, defined as the area and perimeter of labelled lung contour (*Figures 2,3*); (II) lung height defined as the height of lung bounding rectangle (*Figure 3A-3C*); (III) lung width defined as the width of lung bounding rectangle (*Figure 3A-3C*); (IV) aspect ratio defined as the ratio of width to height of bounding rectangle; (V) extent defined as ratio of lung contour area to bounding rectangle area, calculated by Eq. [1]; (VI) solidity defined as the ratio of lung contour area to its convex hull area, while convex hull of a sample of points is defined as the smallest polygon that connects the outermost points in the given sample (i.e.,

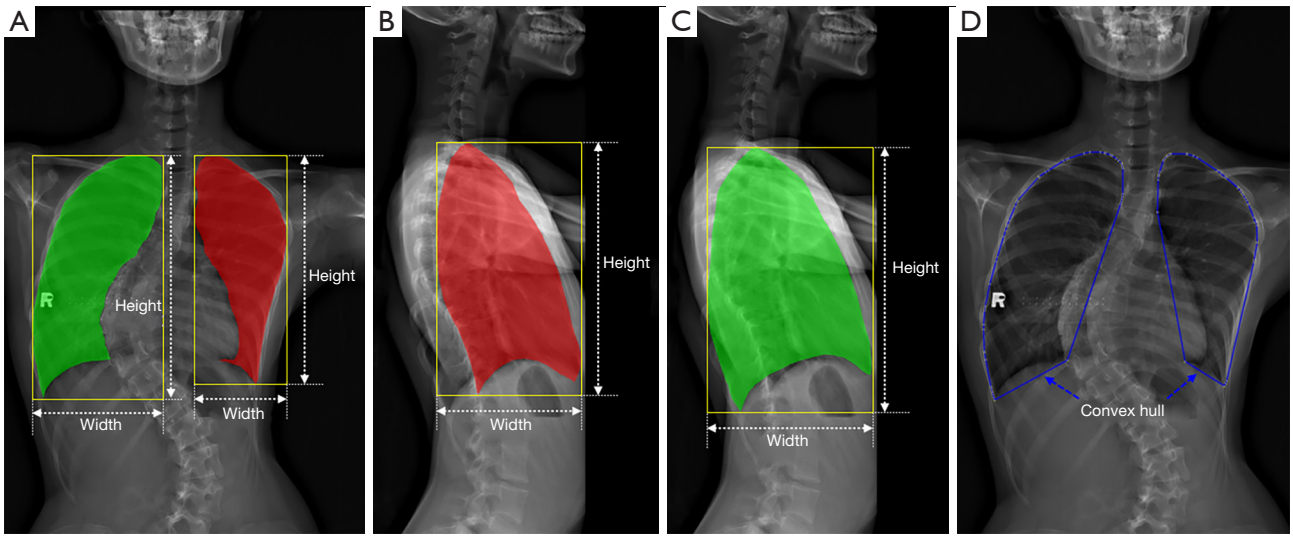

Figure 3 EOS-derived lung geometric measurements. A bounding box (yellow box) and a convex hull (blue polygon) for lung contour are automatically generated for subsequent morphological measurements. Bounding box is defined by the smallest rectangle with vertical and horizontal sides that completely surrounds an object of interest (i.e., labelled lung). All portions of the labelled lung lie within the bounding rectangle (red mask: left lung; green mask: right lung). Convex hull is defined by the smallest polygon that connects the convex points (yellow dots) of the outermost surface of labelled lung. Bounding boxes (yellow rectangles) are automatically drawn on frontal EOS for both left and right lung contour (A), on lateral EOS for left lung contour (B), and on lateral EOS for right lung contour (C), respectively, in conjunction with the convex hulls (blue polygons) of bilateral lung contours on frontal EOS (D). Lung height refers to the height of lung bounding rectangle, while lung width refers to the width of lung bounding rectangle (white dotted line with arrows). The area and perimeter of lung contour (mask) represent the lung area and perimeter. Lung solidity equals to the ratio of lung contour area to its convex hull area. EOS, low-dose biplanar X-ray device.

lung contour), thereby enclosing all points in the sample (25,26) (*Figure 3D*); (VII) equivalent diameter defined as the diameter of the circle which area is identical to lung contour area, computed by Eq. [2].

$$Extent = \frac{Contour\ area}{Boundary\ rectangle\ area} \quad [1]$$

$$Equivalent\ diameter = \frac{\sqrt{4 \times Contour\ area}}{\pi} \quad [2]$$

PF tests (PFTs)

All subjects underwent standard PFTs before PSF, as part of preoperative assessment according to our institutional protocol. PF parameters were calculated by whole-body plethysmography (SensorMedics 6200) and expressed as absolute values (liters) and percentage of predicted values, controlling for body temperature, atmospheric pressure and saturation with water vapor (3). The main measurements included forced vital capacity (FVC and %FVC), forced expiratory volume in 1 second (FEV_1 and $\%FEV_1$), total lung capacity (TLC and %TLC), vital capacity (VC and %VC), residual volume (RV and %RV), and functional residual capacity (FRC and %FRC).

Based on American Thoracic Society criteria, the preoperative PF was stratified into four levels (27,28): (I) normal respiratory function (FVC and FEV_1 ≥80% of predicted value); (II) mild impairment (FVC or FEV_1 =60% to 79% of predicted value), without diminishing ability to perform normal work; (III) moderate impairment (FVC =50% to 59% of predicted value, or FEV_1 =41% to 59% of predicted value), sufficient to diminish ability required for normal work; (IV) severe impairment (FVC <50% or FEV_1 ≤40% of predicted value).

Statistical analysis

The normal distribution of data was proved by Shapiro-Wilk test. For continuous variables with skewed or

Table 1 Preoperative PFTs in 25 AIS patients

Measurement	Impaired PF (n=13)	Normal PF (n=12)
Cobb angle	61.9 [45–92]	60.5 [48–76]
FVC (L)	2.1 [1.6–2.7]	2.8 [2.0–3.6]
FVC pred %	64.1 [52–75]	94.3 [82–118]
FEV_1 (L)	1.8 [1.0–2.3]	2.4 [1.7–3.2]
FEV_1 pred %	59.4 [37–76]	88.8 [72–122]
VC (L)	2.1 [1.6–2.7]	2.8 [2.0–3.7]
VC pred %	64.7 [52–81]	98.0 [73–129]
TLC (L)	3.4 [2.6–4.1]	4.0 [2.6–5.0]
TLC pred %	78.0 [63–93]	99.1 [78–120]
RV (L)	1.3 [0.7–1.8]	1.1 [0.6–1.9]
RV pred %	121.5 [74–191]	115.1 [70–217]
FRC (L)	2.0 [1.3–2.7]	1.9 [1.2–2.8]
FRC pred %	75.6 [15–109]	90.0 [62–138]

Values are expressed as mean [range]. PFTs, pulmonary function tests; AIS, adolescent idiopathic scoliosis; PF, pulmonary function; FVC, forced vital capacity; pred, predicted value; FEV_1, forced expiratory volume in 1 second; VC, vital capacity; TLC, total lung capacity; RV, residual volume; FRC, functional residual capacity.

unknown distribution, data were presented as median with interquartile range; otherwise, for continuous variables with normal distribution, data were presented as mean ± standard deviation (SD). Paired *t*-test was used for intergroup comparison of normally distributed variables. The Wilcoxon signed-rank test was performed to compare the morphological difference between the groups pre-operatively to post-operatively, and to 1Y-FU. ICCs were calculated to determine the reliability of geometric measurements. All statistical analyses were performed using SPSS 26.0 (Armonk, NY, USA). Statistical tests were two-sided with the significance level set to P<0.05.

Results

The study cohort included a total of 25 AIS female patients (age range: 13–31 years; mean: 18 years) with a predominant right-sided thoracic curve (standing Cobb angle range: 45° to 92°; mean: 61.2°). EOS images enabled the satisfactory delineation of lung boundary, in virtue of distinct grayscale/intensity contrast between lung and adjacent organs/structures, like spinal column, diaphragm, and mediastinum. Surgical procedures in all patients were uneventful without significant complications. We analyzed the test results of 25 AIS patients at pre-operative, post-operative, and 1Y-FU stages (as shown in flow diagram in Figure S1).

Clinical and curve characteristics

The mean Cobb angle significantly reduced from 61.2° (SD: 11.3°) preoperatively to 23.2° (SD: 8.3°) postoperatively (P<0.001), and to 22.9° (SD: 8.9°) at 1Y-FU (P<0.001). Cobb angle was similar between post-operative and 1Y-FU stage (P=0.89). Among all AIS patients, 24 female patients (96%) had already undergone menarche prior to preoperative EOS (age at menarche: 9.0 to 14.4 years), except 1 premenarcheal patient.

Preoperative PFTs results in AIS are listed in *Table 1*. Out of 25 AIS patients, 12 patients (48%) had normal PF, whose pred % FVC ranged from 82–118 (mean: 94.3) and pred % FEV_1 ranged from 72–122 (mean: 88.8). The restrictive PF dysfunction occurred in 13 (52%) patients, comprising of 6 mildly (24%), 6 moderately (24%), and 1 (4%) severely impaired patient. In impaired PF group, FVC pred % fell to below 80 (range: 52–75, mean: 64.1), FEV_1 pred % synchronously decreased to a value lower than 80 (range: 37–76; mean: 59.4).

EOS-derived lung morphologic measurements

The ICCs for the intra-observer reliability of lung geometric measurements are shown in (*Table 2*). The intra-observer reliability was excellent at frontal view (ICC range: 0.908–0.990) and good-to-excellent at lateral view (ICC range: 0.800–0.937) for lung area, height, perimeter, width, aspect ratio, and equivalent diameter. For lung extent and solidity, the reliability was good to excellent at frontal view (ICC range: 0.803–0.917) and moderate at lateral view (ICC range: 0.677–0.729). Lung geometric features derived from EOS images in 25 AIS patients underwent spinal fusion surgery are summarized in *Table 3* for frontal view and in *Table 4* for lateral view, respectively.

Lung area

At frontal view, the median area of left lung demonstrated a considerably increase at both post-operative (104.7 *vs.* 125.1 cm^2; P<0.001) and 1Y-FU stage (104.7 *vs.* 124.5 cm^2; P<0.001), whereas left lung area at 1Y-FU did not exhibit a continuous increase when compared with postoperative value (P=0.84). However, the increment in right lung

Table 2 ICC for intra-observer reliability of lung geometric features in AIS

Geometric feature	Frontal view		Lateral view	
	Preop ICC (95% CI)	Postop ICC (95% CI)	Preop ICC (95% CI)	Postop ICC (95% CI)
Area	0.939 (0.854–0.975)	0.970 (0.927–0.988)	0.862 (0.684–0.943)	0.889 (0.746–0.954)
Height	0.925 (0.670–0.976)	0.908 (0.222–0.977)	0.930 (0.770–0.975)	0.892 (0.590–0.963)
Perimeter	0.972 (0.903–0.990)	0.945 (0.814–0.981)	0.876 (0.715–0.949)	0.800 (0.533–0.918)
Width	0.990 (0.974–0.996)	0.946 (0.870–0.978)	0.884 (0.736–0.952)	0.907 (0.780–0.962)
Aspect ratio	0.975 (0.901–0.992)	0.952 (0.787–0.984)	0.902 (0.770–0.960)	0.937 (0.844–0.975)
Equivalent diameter	0.947 (0.872–0.979)	0.969 (0.926–0.988)	0.862 (0.684–0.943)	0.890 (0.748–0.955)
Extent	0.852 (0.627–0.942)	0.917 (0.912–0.971)	0.725 (0.354–0.889)	0.669 (0.341–0.853)
Solidity	0.821 (0.609–0.925)	0.803 (0.572–0.917)	0.677 (0.343–0.859)	0.729 (0.429–0.884)

ICC, intraclass correlation coefficient; AIS, adolescent idiopathic scoliosis; CI, confidence interval.

area was minor without statistically significant differences (median: 143.8, 146.5, 148.4 cm^2 at pre-operative, post-operative, 1Y-FU stage, respectively; all P>0.05) (*Figure 4A*). The mean increase ratio of area at 1Y-FU was 17.4% in the left lung, greater than 5.7% in the right lung.

At lateral view, the increase in left lung area was slight without statistically significant differences (median: 175.8, 178.4, 182.5 cm^2 at pre-operative, post-operative, 1Y-FU stage, respectively; all P>0.05). The right lung area did not significantly change postoperatively (median: 209.9, 206.7, 212.4 cm^2 at pre-operative, post-operative, 1Y-FU stage, respectively; all P>0.05) (*Figure 4B*).

Lung height

For left lung height at frontal view, the absolute value increased significantly from a median of 21.2 cm preoperatively to a median of 23.5 cm postoperatively (P<0.001); however, there was no significant difference between post-operative and 1Y-FU stage (median: 23.5 *vs.* 23.5 cm; P=0.11). For right lung height at frontal view, the preoperative value was not significantly different from postoperative or 1Y-FU value (median: 23.4, 23.2, 23.7 cm at pre-operative, post-operative, 1Y-FU stage, respectively; all P>0.05) (*Figure 4C*). The mean increase ratio of height at 1Y-FU in left lung was higher than that in right lung (13.3% *vs.* 3.2%).

At lateral view, left lung height increased significantly from a median of 22.8 cm preoperatively to a median of 23.8 cm postoperatively (P=0.03); however, there was no statistically significant difference between postoperative and 1Y-FU stage (median: 23.8 *vs.* 23.9 cm; P=0.81). Preoperative right lung height did not differ significantly from either postoperative (24.3 *vs.* 23.4 cm; P=0.2) or 1Y-FU value (24.3 *vs.* 24.9 cm; P=0.07). A slight increase in right lung height was observed from postoperative to 1Y-FU stage (23.4 *vs.* 24.9 cm; P=0.02) (*Figure 4D*). The mean increase ratio of height at 1Y-FU was more pronounced in left lung than in right lung (7.8% *vs.* 3.0%).

Other lung geometric features

At frontal view, the above significant increasing trend in left lung height, starting from an immediate increased value postoperatively (P<0.001) and then keeping unchanged at 1Y-FU statistically, was revealed in left lung for median equivalent diameter (from 11.5 to 12.6 and to 12.6 cm) and median perimeter (from 52.3 to 58.2 and to 58.7 cm), while in right lung for median solidity (from 0.829 to and to 0.892 and to 0.906) and median extent (from 0.513 to 0.669 and to 0.648) (*Table 3*).

The left lung width at frontal view significantly increased at either postoperative (median: 8.5 *vs.* 9.2 cm; P<0.001) or 1Y-FU stage (median: 8.5 *vs.* 9.1 cm^2; P=0.003), while a decline in right lung width was displayed at postoperative and 1Y-FU stage (P<0.001) (*Table 3*). At lateral view, the lung width after operation was significantly reduced than that before operation in bilateral lung (P<0.05), followed with a rebound at 1Y-FU (*Table 4*).

At frontal view, there were no significant interval changes in solidity of left lung, as well as in equivalent diameter of right lung (all P>0.05) (*Table 3*). At lateral view, no

Table 3 Preoperative and postoperative lung geometric features derived from EOS data in 25 AIS patients underwent spinal fusion surgery (frontal view)

Measurement	Preop (A) (n=25)	Postop (B) (n=25)	1Y-FU (C) (n=25)	% change ratio (A *vs*. C)	P value (A *vs*. B)	P value (A *vs*. C)	P value (B *vs*. C)
Cobb angle (°)	61.2 (11.3)	23.2 (8.3)	22.9 (8.9)	–61.3 (10.5)	<0.001#	<0.001#	0.89
Area (cm^2)							
Right lung	143.8 (126.6–158.0)	146.5 (127.1–163.1)	148.4 (128.0–170.3)	5.7 (14.9)	0.76	0.13	0.19
Left lung	104.7 (96.9–127.3)	125.1 (109.1–142.8)	124.5 (107.8–146.1)	17.4 (13.2)	<0.001*	<0.001*	0.84
Aspect ratio							
Right lung	0.543 (0.501–0.576)	0.423 (0.404–0.462)	0.426 (0.400–0.474)	–19.0 (9.0)	<0.001*	<0.001*	0.68
Left lung	0.404 (0.389–0.432)	0.396 (0.349–0.456)	0.400 (0.37–0.415)	–5.2 (9.0)	0.99	0.01*	0.14
Equivalent diameter (cm)							
Right lung	13.5 (12.7–14.2)	13.7 (12.7–14.4)	13.7 (12.8–14.7)	–2.6 (7.1)	0.76	0.15	0.22
Left lung	11.5 (11.1–12.7)	12.6 (11.8–13.5)	12.6 (11.7–13.6)	8.2 (6.0)	<0.001*	<0.001*	0.80
Extent							
Right lung	0.513 (0.469–0.545)	0.669 (0.616–0.693)	0.648 (0.587–0.666)	23.5 (14.2)	<0.001*	<0.001*	0.07
Left lung	0.600 (0.570–0.623)	0.594 (0.536–0.616)	0.589 (0.550–0.611)	–3.1 (5.8)	0.11	0.02*	0.70
Height (cm)							
Right lung	23.4 (21.7–24.2)	23.2 (21.2–24.7)	23.7 (21.5–25.3)	3.2 (8.2)	0.97	0.13	0.05
Left lung	21.2 (19.4–22.3)	23.5 (21.9–25.0)	23.5 (22.7–25.3)	13.3 (8.2)	<0.001*	<0.001*	0.11
Perimeter (cm)							
Right lung	63.7 (58.1–65.7)	59.3 (55.4–62.9)	60.0 (55.8–63.7)	–2.6 (5.9)	<0.001*	0.01*	0.16
Left lung	52.3 (50.3–56.2)	58.2 (56.3–62.0)	58.7 (56.1–61.1)	11.9 (7.4)	<0.001*	<0.001*	0.53
Solidity							
Right lung	0.829 (0.763–0.891)	0.892 (0.878–0.919)	0.906 (0.888–0.916)	9.0 (7.4)	<0.001*	<0.001*	0.33
Left lung	0.890 (0.855–0.936)	0.895 (0.866–0.919)	0.894 (0.870–0.913)	0.4 (4.6)	0.80	0.78	0.78
Width (cm)							
Right lung	12.6 (11.4–13.2)	9.8 (9.2–10.3)	10.1 (9.4–10.7)	–16.9 (6.8)	<0.001*	<0.001*	0.04*
Left lung	8.5 (8.1–9.0)	9.2 (8.7–9.6)	9.1 (8.7–10.0)	7.2 (9.9)	<0.001*	0.003*	0.35

Values are expressed as median with interquartile range (25^{th} percentile to 75^{th} percentile) unless otherwise indicated. Cobb angle and change ratio are expressed as mean (SD). *, Wilcoxon signed-rank test: P<0.05; #, paired *t*-test: P<0.05. EOS, low-dose biplanar X-ray device; AIS, adolescent idiopathic scoliosis; 1Y-FU, 1-year follow up; SD, standard deviation.

significant interval changes were indicated in aspect ratio of right lung, as well as in equivalent diameter of bilateral lung (all P>0.05) (*Table 4*).

Discussion

The most compelling advantage of EOS imaging, categorized into standard low-dose and micro-dose protocol, consists in the substantial reduction in radiation exposure (29-32). For whole spine radiographs, low-lose EOS allows a dose-area product approximately 50% less than digital radiography (DR) (30), and only produces 6 to 9 times less skin entrance dose than conventional computed radiography (CR) (31). The radiation dose exposure of a single full-spine examination is approximately 6 to 7 times lower from micro-dose EOS than from low-dose EOS,

Table 4 Preoperative and postoperative lung geometric features derived from EOS data in 25 AIS patients underwent spinal fusion surgery (lateral view)

Measurement	Preop (A) (n=25)	Postop (B) (n=25)	1Y-FU (C) (n=25)	% change ratio (A *vs*. C)	P value (A *vs*. B)	P value (A *vs*. C)	P value (B *vs*. C)
Area (cm^2)							
Right lung	209.9 (196.1–240.9)	206.7 (191.1–235.3)	212.4 (200.5–246.8)	3.3 (13.9)	0.24	0.24	0.06
Left lung	175.8 (169.6–186.2)	178.4 (160.6–205.3)	182.5 (169.2–208.5)	5.0 (12.9)	0.66	0.18	0.40
Aspect ratio							
Right lung	0.613 (0.525–0.635)	0.573 (0.524–0.683)	0.586 (0.512–0.633)	–2.0 (14.3)	0.88	0.16	0.33
Left lung	0.561 (0.507–0.667)	0.490 (0.434–0.623)	0.506 (0.472–0.586)	–9.5 (11.6)	<0.01*	<0.001*	0.84
Equivalent diameter (cm)							
Right lung	16.3 (15.8–17.5)	16.2 (15.6–17.3)	16.4 (16.0–17.7)	1.4 (7.0)	0.23	0.28	0.07
Left lung	15.0 (14.7–15.4)	15.1 (14.3–16.2)	15.2 (14.7–16.3)	2.3 (6.2)	0.07	0.17	0.35
Extent							
Right lung	0.627 (0.587–0.665)	0.666 (0.630–0.691)	0.639 (0.600–0.648)	0.2 (8.5)	<0.01*	0.86	<0.01*
Left lung	0.631 (0.589–0.670)	0.659 (0.630–0.696)	0.642 (0.607–0.652)	0.7 (8.9)	0.02*	0.84	0.01*
Height (cm)							
Right lung	24.3 (22.8–25.5)	23.4 (21.9–25.9)	24.9 (22.7–26.7)	3.0 (7.7)	0.20	0.07	0.02*
Left lung	22.8 (21.6–23.3)	23.8 (21.7–26.1)	23.9 (22.5–25.6)	7.8 (9.0)	0.03*	<0.001*	0.81
Perimeter (cm)							
Right lung	67.6 (63.2–70.6)	65.9 (62.8–69.2)	69.8 (62.7–72.0)	1.5 (6.4)	0.15	0.22	<0.01*
Left lung	62.4 (59.1–64.0)	65.0 (61.0–68.0)	64.1 (61.1–68.9)	4.2 (7.2)	0.14	0.01*	0.66
Solidity							
Right lung	0.909 (0.884–0.930)	0.925 (0.906–0.941)	0.921 (0.898–0.928)	1.0 (4.6)	0.02*	0.51	<0.01*
Left lung	0.924 (0.903–0.932)	0.922 (0.907–0.940)	0.922 (0.912–0.932)	4.2 (7.2)	0.02*	0.33	0.99
Width (cm)							
Right lung	14.3 (12.7–15.9)	13.7 (12.4–15.1)	14.2 (12.8–15.6)	0.4 (12.2)	0.02*	0.93	0.03*
Left lung	12.4 (11.6–14.4)	11.5 (10.7–13.0)	12.4 (11.1–13.6)	–3.0 (8.9)	<0.001*	0.06	0.05

Values are expressed as median with interquartile range (25^{th} percentile to 75^{th} percentile) unless otherwise indicated. Change ratio are expressed as mean (SD). *, Wilcoxon signed-rank test: P<0.05. EOS, low-dose biplanar X-ray device; AIS, adolescent idiopathic scoliosis; 1Y-FU, 1-year follow up; SD, standard deviation.

equivalent to <1-week of natural background radiation exposure (21). The effective dose in micro-dose protocol for adolescents is reduced almost 17 times as compared to CR system (21). When substituted for CT on measurement of femoral and tibial torsion, EOS delivers remarkably lower dose of ionizing radiation to organs, as reflected by 4.1-fold reduction for ovaries, 24-fold reduction for testicles, and 13–30-fold reduction for the knees and ankles (32). The prospective use of serial CT scanning for depicting lung morphology is not advocated, on account of its high radiation exposure (8,33). EOS-derived lung morphology assessment circumvents many of the obstacles pertinent to concerns raised by irradiation risk. Therefore, we were able to approach the serial changes of lung morphology, without posing considerable radiation burden to subjects. The results of current study may reinforce the usefulness of EOS in AIS imaging.

EOS technique also grabs attention of researchers

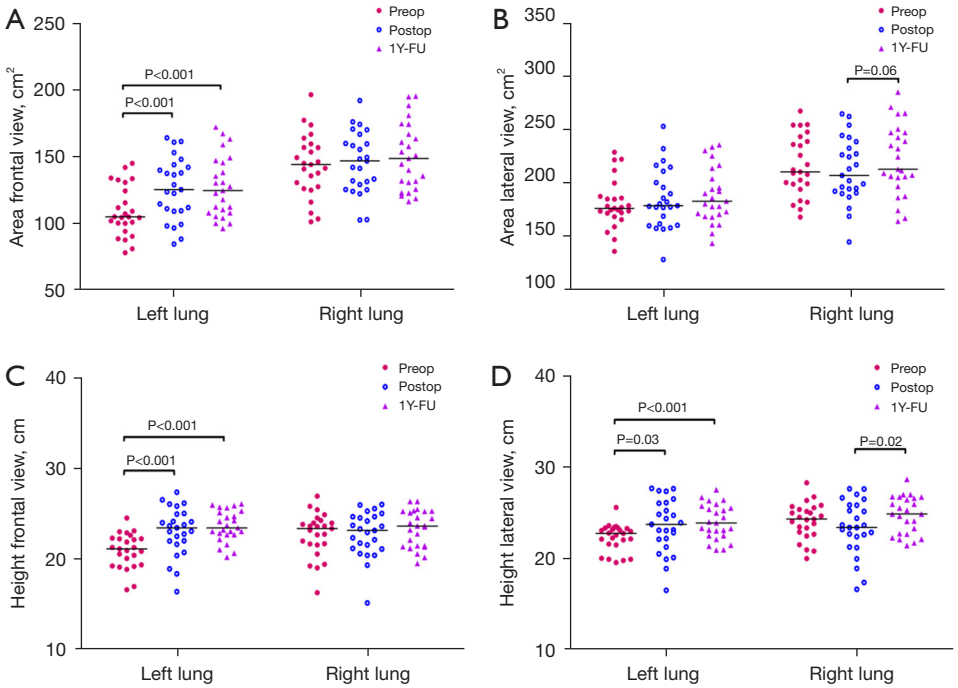

Figure 4 Group comparisons of EOS-derived bilateral lung geometric features. (A) At frontal view, left lung area significantly increases at both post-operative and 1Y-FU stage, whereas right lung area demonstrates a slight but insignificant interval increase. (B) At lateral view, the increase in left lung area is slight without statistically significant difference, and right lung area does not significantly change postoperatively. (C,D) At both frontal and lateral view, left lung height significantly improves at either post-operative or 1Y-FU stage, while preoperative right lung height is not significantly different from postoperative and 1Y-FU value. EOS, low-dose biplanar X-ray device; 1Y-FU, 1-year follow-up.

for its desirable 3D statistical modelling available for spine, hip, knee, rib cage, in terms of high reliability and reproducibility, accuracy (13-15,34,35). Humbert *et al.* demonstrated that EOS-3D modelling could yield not only the average shape accuracy of 1.0 mm in comparison with CT, but also satisfactory precision of 3D-reconstruction method both for vertebrae position (1.8 mm) and orientation (2.3°–3.9°) (14). In present study, for the vast majority of 2D lung geometric features, an excellent measure-remeasure reliability was garnered at frontal view, coupled with a good-to-excellent reliability at lateral view. EOS-derived lung morphology was acquired during breath-holding at static status rather than dynamic (inspiratory and expiratory) phrase, eliminating the measurement discrepancy that might arise from diaphragm motion during deep inspiration/expiration episodes. This was partially substantiated by the good-to-excellent measurement reliability.

To date, it remains unclear how lung morphology changes in response to surgical correction. Our EOS-based morphological data demonstrated a markedly improvement in lung area as well as concomitant increase in lung height after spinal fusion surgery in AIS. We surmise that the increase in lung area and height is probably attributable to the restoration in shape and symmetry of thoracic cage. The less distorted configuration of thoracic cage is thought to lessen the mechanic restriction to lung motion during respiration. The remodelling of the chest after surgery usually results in the reestablishment of thoracic cavity symmetry (i.e., elevated hemithoracic symmetry ratio), as well as the corrected deformity of ribs and spinal components at sagittal, axial, coronal planes, which may jointly contribute to an improvement in expansibility, mobility, and kinematics of chest wall (8,33,36,37). This could ultimately diminish the restriction and increase the maximum amplitude for lung motion, enabling a larger expansion of lung capacity.

The natural growth of lung usually experiences a “golden stage” between birth and 8 years of age, coinciding with development of spinal column and thoracic cage (38),

during which a sharp rise in lung parenchyma volume represents a function of age (10). Reflected by 3D volumetric reconstruction of 1,050 normal CT data, lung parenchyma growth starts from approximately 400 cc at birth to around 900 to 1,500 cc at age of 5–10 years, and reaches to 4,500 cc for males and 3,500 for females at skeletal maturity (10). During adolescence, lung growth pattern is quite different between females and males (39,40). In a cross-sectional study in adolescents, in 51 girls aged 13 to 18 years, lung growth was nearly finished soon after the menarche. By contrast, in 52 age-matched boys, lung development persisted during and till the end of puberty (40). In a longitudinal study involving 626 adolescents aged 11.5 to 18.5 years within 6 years of follow-up, thorax height grew in proportion to thorax width during growth spurt; however, thorax height in males continued to increase, when adult values of thorax width and standing height were gained in females (39). In entire AIS cohort, all but one patient had already undergone menarche before pre-operative EOS, which suggests that observed increase in lung area/height is far less likely to arise from the natural growth of lung parenchyma, resulting from premenarcheal alveolar proliferation and bronchial tree development.

The tendency of left lung area increase demonstrated a distinctive pattern, which was characterized with an immediately increased value postoperatively that persisted to 1Y-FU. Left lung equivalent diameter and perimeter changed in similar pattern, partly due to their mathematically positive correlation with area. The distinctive pattern indicated a plateau between postoperative and 1Y-FU stage in left lung area, which might be attributed to the similarity in thoracic cage disfiguration. There was no further reduction in Cobb angle at 1Y-FU when compared with postoperative stage, indicative of a relatively "static" deformity extent of thoracic cage. This was also in concordance with our speculation, that was, observed lung geometry change was likely not due to the growth in lung parenchyma but instead to the restoration of shape and symmetry of thoracic cage.

Unlike the remarkable increase of left lung area at 1Y-FU, the increase in right lung area was, however, very minor, in accordance with Fujita *et al*. study involving 111 AIS patients underwent PSF, in which the left lung gained more pronounced increase in volume than right lung (41). Also, height gains in left lung exceeded right lung postoperatively. For both lung area and height, their increase ratio at 1Y-FU in left side were apparently higher than that in right side. This phenomenon indicates that, after the diminution of asymmetry and deformity of thoracic cage following spinal fusion, left lung motion is less constrained *vs.* right lung motion, probably leading to the disproportional improvement of lung area between bilateral lungs.

Most of previous AIS studies on lung morphology interrogated the variation of lung volume, with a reliance on CT and MRI assessment. However, there has been debate about whether lung volume increases after scoliosis corrective surgery by far and away. Sarwahi *et al*. demonstrated in a 3D-reconstruction CT study on 29 AIS patients that neither total lung volume nor left/right lung volume ratio changed significantly postoperatively, and as such they conceived of previously-documented improvements in PFTs as a dynamic rather than a static phenomenon (33). Sarwahi *et al*. also concluded that hemithoracic symmetry increased after surgery, demonstrating the reestablishment of chest wall symmetry independent of the change in lung volume. Other investigators disagree and assert that absolute lung volume do increase after deformity correction in AIS (8,41,42). Yu *et al*. observed the significant increase in left lung volume, total volume and hemithoracic ratio 2 years after thoracoscopic anterior spinal fusion (TASF), from 3D CT reconstructed data of 23 AIS patients; nevertheless, the lung volumes post TASF remained in the bottom 50th percentile, relative to thoracically normal female reference data (8). Fujita *et al*. detected a postoperative reduction of left lung volume followed by the increase at 2-year follow up. The discrepancy in fusion area might be accountable for above disparity. Fujita *et al*. speculated that longer fusion might incur postoperative decline in left lung volume, and put forward a spinal fusion length of <11 levels for preserving left lung volume (41). In our earlier comparison study, the individual or total inspiratory and expiratory volume of lung, as measured by dynamic fast breath-hold MRI, displayed slight but insignificant increment after PSF (43). Current study extends prior lung measures depending on supine MRI and CT to EOS-based measures complying with upright biomechanics. The 2D lung morphology variation from EOS cannot be directly translated to any improvements in 3D lung volume. However, current EOS findings are partially in agreement with those CT or MRI evidences indicative of the postoperatively diminished restriction to lung motion leading to greater lung capacity.

The incidence of restrictive pulmonary dysfunction ranges from approximately 20 % to 61% in surgically treated AIS, following the American Thoracic Society

definition of normal PF (FVC and FEV_1 ≥80% of predicted value). Nineteen percent to 41% of severe AIS patients suffer from a clinically relevant degree of impairment of PF, defined as 60% to 65% or less of predicted values for FVC and FEV_1. Almost half of our AIS patients (48%) had normal respiratory function, in line with observations by Sarwahi *et al.* (46%) and Kim *et al.* (41%) (5,33). So far, it continues to be controversial whether scoliosis correction is beneficial to PF, and whether thoracic insufficiency syndrome may occur as a consequence of early spinal fusion procedure. Quite a few researchers have exhibited that scoliosis correction definitely ameliorate PFTs indices (44,45). On the contrary, others disprove and emphasize that PFTs indices return to pre-operative values or even deteriorate, irrespective of surgical approach (46,47). On the other hand, neither underlying thoracic asymmetry nor postoperative symmetry reestablishment can be uncovered by PFTs results alone, in term of hemithoracic width/ratio (8,48). These findings may imply that the capability of PFTs to gauge the effect of scoliosis correction is likely to be limited, and postoperative PFTs has not been incorporated into the routine protocol for follow-up assessment in AIS patients undergoing spinal fusion. Because of a paucity of post-operative PFTs indices, the relationship between lung morphology change and PF variation remains unknown at this moment. Of note, this exerts no influence on the significance of any of our lung morphology results.

The main strengths of the present study lie in the introduction of low-dose EOS imaging into lung morphology assessment, automatic extraction of various lung geometric features, follow-up protocol allowing serial observations for lung morphology, prospective cohort with well-defined inclusion criteria. Several limitations exist in the present study. The sample size was relatively small. Insufficient cohort size is less likely to generate statistically significance, particularly for the latent lung geometric features slightly altered by corrective surgery. However, small sample size appears to be a common limitation in most of similar studies, probably due to the confirmed efficacy and broader application of bracing treatment in preventing curve deterioration, as well as immanent population prevalence of AIS. Besides, potential selection bias was possibly introduced into this single centre study. In this case, we advocate to launch multi-centre study to enlarge the sample size and eliminate the bias. Since our results were obtained shortly after the surgery within 12 months, prolonged duration of follow-up to represent ultimate outcome, is warranted to ascertain the improvement in lung morphology attained from EOS.

Conclusions

EOS imaging demonstrates that left lung area in severe AIS patients may improve after PSF surgery. EOS may provide useful information about lung morphological change in severe AIS after PSF on top of spinal deformity correction.

Acknowledgments

Funding: This work was supported by the General Research Funding from the Research Grants Council of the Hong Kong Special Administrative Region, China (No. CUHK 14206716; No. CUHK 411811).

Footnote

Reporting Checklist: The authors have completed the TREND reporting checklist. Available at https://qims.amegroups.com/article/view/10.21037/qims-21-1147/rc

Conflicts of Interest: All authors have completed the ICMJE uniform disclosure form (available at https://qims.amegroups.com/article/view/10.21037/qims-21-1147/coif). All authors report that this work was supported by the General Research Funding from the Research Grants Council of the Hong Kong Special Administrative Region, China (No. CUHK 14206716; No. CUHK 411811). The authors have no other conflicts of interest to declare.

Ethical Statement: The authors are accountable for all aspects of the work in ensuring that questions related to the accuracy or integrity of any part of the work are appropriately investigated and resolved. The study was conducted in accordance with the Declaration of Helsinki (as revised in 2013). Ethical approval was obtained from The Joint Chinese University of Hong Kong-New Territories East Cluster Clinical Research Ethics Committee (CREC Ref. No. 2013.386 and No. 2016.058). Written informed consent was obtained from study patients or their parent/guardian.

References

1. Weinstein SL, Dolan LA, Cheng JC, Danielsson A, Morcuende JA. Adolescent idiopathic scoliosis. Lancet 2008;371:1527-37.
2. Cheng JC, Castelein RM, Chu WC, Danielsson AJ, Dobbs MB, Grivas TB, Gurnett CA, Luk KD, Moreau A, Newton PO, Stokes IA, Weinstein SL, Burwell RG. Adolescent idiopathic scoliosis. Nat Rev Dis Primers 2015;1:15030.
3. Chu WC, Li AM, Ng BK, Chan DF, Lam TP, Lam WW, Cheng JC. Dynamic magnetic resonance imaging in assessing lung volumes, chest wall, and diaphragm motions in adolescent idiopathic scoliosis versus normal controls. Spine (Phila Pa 1976) 2006;31:2243-9.
4. Tsiligiannis T, Grivas T. Pulmonary function in children with idiopathic scoliosis. Scoliosis 2012;7:7.
5. Kim YJ, Lenke LG, Bridwell KH, Cheh G, Whorton J, Sides B. Prospective pulmonary function comparison following posterior segmental spinal instrumentation and fusion of adolescent idiopathic scoliosis: is there a relationship between major thoracic curve correction and pulmonary function test improvement? Spine (Phila Pa 1976) 2007;32:2685-93.
6. Zhang JG, Wang W, Qiu GX, Wang YP, Weng XS, Xu HG. The role of preoperative pulmonary function tests in the surgical treatment of scoliosis. Spine (Phila Pa 1976) 2005;30:218-21.
7. Newton PO, Faro FD, Gollogly S, Betz RR, Lenke LG, Lowe TG. Results of preoperative pulmonary function testing of adolescents with idiopathic scoliosis. A study of six hundred and thirty-one patients. J Bone Joint Surg Am 2005;87:1937-46.
8. Yu CG, Grant CA, Izatt MT, Labrom RD, Askin GN, Adam CJ, Little JP. Change in Lung Volume Following Thoracoscopic Anterior Spinal Fusion Surgery: A 3-Dimensional Computed Tomography Investigation. Spine (Phila Pa 1976) 2017;42:909-16.
9. Adam CJ, Cargill SC, Askin GN. Computed tomographic-based volumetric reconstruction of the pulmonary system in scoliosis: trends in lung volume and lung volume asymmetry with spinal curve severity. J Pediatr Orthop 2007;27:677-81.
10. Gollogly S, Smith JT, White SK, Firth S, White K. The volume of lung parenchyma as a function of age: a review of 1050 normal CT scans of the chest with three-dimensional volumetric reconstruction of the pulmonary system. Spine (Phila Pa 1976) 2004;29:2061-6.
11. Yazici M, Acaroglu ER, Alanay A, Deviren V, Cila A, Surat A. Measurement of vertebral rotation in standing versus supine position in adolescent idiopathic scoliosis. J Pediatr Orthop 2001;21:252-6.
12. Rehm J, Germann T, Akbar M, Pepke W, Kauczor HU, Weber MA, Spira D. 3D-modeling of the spine using EOS imaging system: Inter-reader reproducibility and reliability. PLoS One 2017;12:e0171258.
13. Glaser DA, Doan J, Newton PO. Comparison of 3-dimensional spinal reconstruction accuracy: biplanar radiographs with EOS versus computed tomography. Spine (Phila Pa 1976) 2012;37:1391-7.
14. Humbert L, De Guise JA, Aubert B, Godbout B, Skalli W. 3D reconstruction of the spine from biplanar X-rays using parametric models based on transversal and longitudinal inferences. Med Eng Phys 2009;31:681-7.
15. Al-Aubaidi Z, Lebel D, Oudjhane K, Zeller R. Three-dimensional imaging of the spine using the EOS system: is it reliable? A comparative study using computed tomography imaging. J Pediatr Orthop B 2013;22:409-12.
16. Pomero V, Mitton D, Laporte S, de Guise JA, Skalli W. Fast accurate stereoradiographic 3D-reconstruction of the spine using a combined geometric and statistic model. Clin Biomech (Bristol, Avon) 2004;19:240-7.
17. Sabourin M, Jolivet E, Miladi L, Wicart P, Rampal V, Skalli W. Three-dimensional stereoradiographic modeling of rib cage before and after spinal growing rod procedures in early-onset scoliosis. Clin Biomech (Bristol, Avon) 2010;25:284-91.
18. Aubert B, Vergari C, Ilharreborde B, Courvoisier A, Skalli W. 3D reconstruction of rib cage geometry from biplanar radiographs using a statistical parametric model approach. Comput Methods Biomech Biomed Eng Imaging Vis 2016;4:281-95.
19. Damet J, Fournier P, Monnin P, Sans-Merce M, Ceroni D, Zand T, Verdun FR, Baechler S. Occupational and patient exposure as well as image quality for full spine examinations with the EOS imaging system. Med Phys 2014;41:063901.
20. Luo TD, Stans AA, Schueler BA, Larson AN. Cumulative Radiation Exposure With EOS Imaging Compared With Standard Spine Radiographs. Spine Deform 2015;3:144-50.

21. Pedersen PH, Petersen AG, Østgaard SE, Tvedebrink T, Eiskjær SP. EOS Micro-dose Protocol: First Full-spine Radiation Dose Measurements in Anthropomorphic Phantoms and Comparisons with EOS Standard-dose and Conventional Digital Radiology. Spine (Phila Pa 1976) 2018;43:E1313-21.
22. Faro FD, Marks MC, Pawelek J, Newton PO. Evaluation of a functional position for lateral radiograph acquisition in adolescent idiopathic scoliosis. Spine (Phila Pa 1976) 2004;29:2284-9.
23. Koo TK, Li MY. A Guideline of Selecting and Reporting Intraclass Correlation Coefficients for Reliability Research. J Chiropr Med 2016;15:155-63.
24. Lempitsky V, Kohli P, Rother C, Sharp T. Image segmentation with a bounding box prior. In: 2009 IEEE 12th international conference on computer vision. IEEE, 2009:277-84.
25. Pulagam AR, Kande GB, Ede VK, Inampudi RB. Automated Lung Segmentation from HRCT Scans with Diffuse Parenchymal Lung Diseases. J Digit Imaging 2016;29:507-19.
26. Kalia RK, Sharma A, Amin SB, Saha M, Thittamaranahalli SK. AI-driven quantification of ground glass opacities in lungs of COVID-19 patients using 3D computed tomography imaging. medRxiv 2021. doi: 10.1101/2021.07.06.21260109.
27. Johnston CE, Richards BS, Sucato DJ, Bridwell KH, Lenke LG, Erickson M; Spinal Deformity Study Group. Correlation of preoperative deformity magnitude and pulmonary function tests in adolescent idiopathic scoliosis. Spine (Phila Pa 1976) 2011;36:1096-102.
28. Evaluation of impairment/disability secondary to respiratory disorders. American Thoracic Society. Am Rev Respir Dis 1986;133:1205-9.
29. EOS imaging Launches EOS 3D Service, a 3D Modeling offering for Customers Worldwide. 2015. Available online: https://www.eos-imaging.com/wp-content/uploads/2015/05/150512_3D_Service_Offering_0.pdf
30. Dietrich TJ, Pfirrmann CW, Schwab A, Pankalla K, Buck FM. Comparison of radiation dose, workflow, patient comfort and financial break-even of standard digital radiography and a novel biplanar low-dose X-ray system for upright full-length lower limb and whole spine radiography. Skeletal Radiol 2013;42:959-67.
31. Deschênes S, Charron G, Beaudoin G, Labelle H, Dubois J, Miron MC, Parent S. Diagnostic imaging of spinal deformities: reducing patients radiation dose with a new slot-scanning X-ray imager. Spine (Phila Pa 1976) 2010;35:989-94.
32. Delin C, Silvera S, Bassinet C, Thelen P, Rehel JL, Legmann P, Folinais D. Ionizing radiation doses during lower limb torsion and anteversion measurements by EOS stereoradiography and computed tomography. Eur J Radiol 2014;83:371-7.
33. Sarwahi V, Sugarman EP, Wollowick AL, Amaral TD, Harmon ED, Thornhill B. Scoliosis surgery in patients with adolescent idiopathic scoliosis does not alter lung volume: a 3-dimensional computed tomography-based study. Spine (Phila Pa 1976) 2014;39:E399-405.
34. Machino M, Kawakami N, Ohara T, Saito T, Tauchi R, Imagama S. Accuracy of rib cage parameters from 3-Dimensional reconstruction images obtained using simultaneous biplanar radiographic scanning technique in adolescent idiopathic scoliosis: Comparison with conventional computed tomography. J Clin Neurosci 2020;75:94-8.
35. Bagheri A, Liu XC, Tassone C, Thometz J, Tarima S. Reliability of Three-Dimensional Spinal Modeling of Patients With Idiopathic Scoliosis Using EOS System. Spine Deform 2018;6:207-12.
36. Picetti GD 3rd, Ertl JP, Bueff HU. Endoscopic instrumentation, correction, and fusion of idiopathic scoliosis. Spine J 2001;1:190-7.
37. Takahashi S, Suzuki N, Asazuma T, Kono K, Ono T, Toyama Y. Factors of thoracic cage deformity that affect pulmonary function in adolescent idiopathic thoracic scoliosis. Spine (Phila Pa 1976) 2007;32:106-12.
38. Dimeglio A, Canavese F. The growing spine: how spinal deformities influence normal spine and thoracic cage growth. Eur Spine J 2012;21:64-70.
39. DeGroodt EG, van Pelt W, Borsboom GJ, Quanjer PH, van Zomeren BC. Growth of lung and thorax dimensions during the pubertal growth spurt. Eur Respir J 1988;1:102-8.
40. Nève V, Girard F, Flahault A, Boulé M. Lung and thorax development during adolescence: relationship with pubertal status. Eur Respir J 2002;20:1292-8.
41. Fujita N, Yagi M, Michikawa T, Yamada Y, Suzuki S, Tsuji O, Nagoshi N, Okada E, Tsuji T, Nakamura M, Matsumoto M, Watanabe K. Impact of fusion for adolescent idiopathic scoliosis on lung volume measured with computed tomography. Eur Spine J 2019;28:2034-41.
42. Fu J, Liu C, Zhang YG, Zheng GQ, Zhang GY, Song K, Tang XY, Wang Y. Three-dimensional computed tomography for assessing lung morphology in adolescent idiopathic scoliosis following posterior spinal fusion

surgery. Orthop Surg 2015;7:43-9.
43. Chu WC, Ng BK, Li AM, Lam TP, Lam WW, Cheng JC. Dynamic magnetic resonance imaging in assessing lung function in adolescent idiopathic scoliosis: a pilot study of comparison before and after posterior spinal fusion. J Orthop Surg Res 2007;2:20.
44. Kinnear WJ, Johnston ID. Does Harrington instrumentation improve pulmonary function in adolescents with idiopathic scoliosis? A meta-analysis. Spine (Phila Pa 1976) 1993;18:1556-9.
45. Lenke LG, Bridwell KH, Baldus C, Blanke K. Analysis of pulmonary function and axis rotation in adolescent and young adult idiopathic scoliosis patients treated with Cotrel-Dubousset instrumentation. J Spinal Disord 1992;5:16-25.
46. Vedantam R, Lenke LG, Bridwell KH, Haas J, Linville DA. A prospective evaluation of pulmonary function in patients with adolescent idiopathic scoliosis relative to the surgical approach used for spinal arthrodesis. Spine (Phila Pa 1976) 2000;25:82-90.
47. Kinnear WJ, Kinnear GC, Watson L, Webb JK, Johnston ID. Pulmonary function after spinal surgery for idiopathic scoliosis. Spine (Phila Pa 1976) 1992;17:708-13.
48. Campbell RM Jr, Smith MD, Mayes TC, Mangos JA, Willey-Courand DB, Kose N, Pinero RF, Alder ME, Duong HL, Surber JL. The characteristics of thoracic insufficiency syndrome associated with fused ribs and congenital scoliosis. J Bone Joint Surg Am 2003;85:399-408.

Cite this article as: Deng M, Chen Q, Deng Q, Shi L, Cheng CCN, Yeung KH, Zhang R, Yu WPF, Lam TP, Cheng JCY, Chu WCW. Statistical changes of lung morphology in patients with adolescent idiopathic scoliosis after spinal fusion surgery—a prospective nonrandomized study based on low-dose biplanar X-ray imaging. Quant Imaging Med Surg 2022;12(6):3325-3339. doi: 10.21037/qims-21-1147

Supplementary

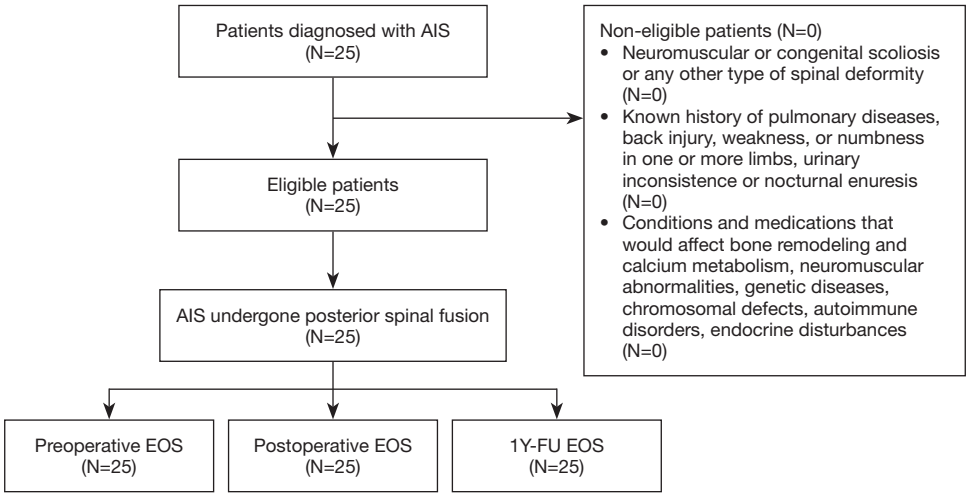

Figure S1 Flow diagram illustrating enrollment and assignment of eligible study participants. AIS, adolescent idiopathic scoliosis; EOS, low-dose biplanar X-ray device; 1Y-FU, 1-year follow up.

https://dx.doi.org/10.21037/qims-21-1147